Heliyon

Received:
2 November 2018
Revised:
15 January 2019
Accepted:
5 February 2019

Cite as: Goki Tamura, Kotaro Kojima, Izuru Takewaki. Critical response of elastic-plastic SDOF systems with nonlinear viscous damping under simulated earthquake ground motions. Heliyon 5 (2019) e01221. doi: 10.1016/j.heliyon.2019.e01221

Critical response of elastic-plastic SDOF systems with nonlinear viscous damping under simulated earthquake ground motions

Goki Tamura [a], **Kotaro Kojima** [b], **Izuru Takewaki** [a,*]

[a] *Department of Architecture and Architectural Engineering, Graduate School of Engineering, Kyoto University, Kyotodaigaku-Katsura, Nishikyo, Kyoto, 615-8540, Japan*

[b] *Faculty of Design and Architecture, Kyoto Institute of Technology, Matsugasaki, Sakyo, Kyoto, 606-8585, Japan*

[*] Corresponding author.

E-mail address: takewaki@archi.kyoto-u.ac.jp (I. Takewaki).

Abstract

Multi impulse with constant time interval is used as a representative of a long-duration earthquake ground motion. An analytical expression is derived for the elastic-plastic response of a single-degree-of-freedom (SDOF) model with nonlinear viscous damping subjected to the "critical multi impulse" which maximizes the response. The fact that only free vibration appears under such multi impulse enables the smart application of an energy approach in deriving the analytical expression for a complicated elastic-plastic response with nonlinear viscous damping. The nonlinear viscous damping characteristic for deformation is approximated in terms of a quadratic or elliptical function. The critical timing of the impulses is found to correspond to the zero restoring-force timing or the maximum velocity timing depending on the input level. It is shown that the nonlinearity in viscous damping causes a remarkable influence on the earthquake response in some cases. The reliability and accuracy of the proposed theory are investigated through the comparison with the results by the time-history response

https://doi.org/10.1016/j.heliyon.2019.e01221

analysis to the tuned sine wave as a representative of the long-duration earthquake ground motion.

Keywords: Civil engineering, Natural hazards, Structural engineering

1. Introduction

Historically near-fault ground motions and long-period, long-duration ground motions caused serious damage to building structures. Some representative near-fault ground motions were observed during Parkfield earthquake in 1966, San Fernando earthquake in 1971, Northridge earthquake in 1994, Hyogoken-nanbu earthquake in 1995, Chi-Chi earthquake in 1999, Niigata-ken Chuetsu earthquake in 2004 and Kumamoto earthquake in 2016. On the other hand, the long-period, long-duration ground motions were observed during Mexico earthquake in 1985, Tokachi-oki earthquake in 2003, Niigata-ken Chuetsu earthquake in 2004 and Tohoku earthquake in 2011 (Takewaki et al., 2011, 2012). It should be pointed out that the long-period, long-duration ground motions were not supposed in the earthquake resistant design of super high-rise buildings about 50 years ago and many serious damages due to this type of ground motions were observed. Many buildings, especially 6 to 15-story buildings were seriously damaged by long-period ground motions which lasted more than 2 minutes during Mexico earthquake in 1985 (Beck and Hall, 1986). The sloshing by the long-period, long-duration ground motions were observed during Tokachi-oki earthquake in 2003 (Hatayama et al., 2004; Aoi et al., 2018) and oil storage tanks were seriously damaged in Tomakomai city about 250 km from the epicenter. In Tokyo, high-rise buildings in resonance with the long-period ground motion lasted over 5 minutes during 2004 Niigata-ken Chuetsu earthquake and their elevator cables were damaged (Furumura and Hayakawa, 2007; Kubo et al., 2009). Rather recently, many records of remarkable long-period, long-duration ground motions were observed in Tokyo and Osaka during Tohoku earthquake in 2011. Some of high-rise buildings in Tokyo and Osaka were in resonance with these ground motions and lasted more than 10 minutes (Takewaki et al., 2011, 2012). Furthermore, the damages of lead dampers in base-isolation stories and pile foundations were observed under these long-duration ground motions during 2011 Tohoku earthquake (Motosaka and Mitsuji, 2012). It seems important to investigate the resonance phenomenon for the structural design of buildings with long natural periods, e.g. high-rise buildings and base-isolated buildings.

A large number of theoretical studies on steady-state response of an elastic-plastic system under the harmonic wave have been accumulated in the last several decades (Caughey, 1960a, b; Iwan, 1961, 1965a, b; Roberts and Spanos, 1990; Liu, 2000). First of all, Caughey (1960a) opened the door in this field. A resonance curve was

https://doi.org/10.1016/j.heliyon.2019.e01221

derived for a single-degree-of-freedom (SDOF) bilinear hysteretic model by taking advantage of the equivalent linearization method based on a least squares approximation. Subsequently, the exact solution for an undamped bilinear hysteretic SDOF model with a positive post-yield stiffness ratio was obtained by Iwan (1961, 1965a) for the harmonic and square waves. The resonant response has to be analyzed for a specific acceleration amplitude by changing the input frequency in a parametric manner and this procedure is too complicated. Furthermore, these theories are only targeted for undamped models or models with linear viscous damping. On the other hand, Kojima and Takewaki (2015a, b, 2016) introduced a new approach to transform the one-cycle and 1.5-cycle sine waves to the double and triple impulses. It is well known that these two waves represent the principal parts of the fault-parallel (fling-step) and fault-normal (forward directivity) components of the near-fault ground motion. Then, Kojima and Takewaki (2015a, b, 2016) derived the critical elastic-plastic responses in closed-form for such double and triple impulses. Multi impulse has also been introduced as a substitute for a multi-cycle sine wave representing the main part of a long-duration ground motion, and closed-form critical steady-state responses have been derived by Kojima and Takewaki (2015c, 2017) for an undamped elastic perfectly-plastic SDOF model and an undamped bilinear hysteretic SDOF model. They demonstrated that the nonlinear response under the multi impulse can be described in terms of free vibrations. Then they derived a closed-form plastic deformation amplitude for the critical multi impulse by taking advantage of the energy balance law. It should be pointed out that their approach does not need to solve the equation of motion directly. These theories using double and multi impulses are expanded for the elastic-plastic model with linear viscous damping (Kojima et al., 2017; Hayashi et al., 2018, Akehashi et al., 2018), the elastic-plastic 2DOF model (Taniguchi et al., 2016) and the elastic-plastic base-isolated building model (Fujita et al., 2017; Takewaki et al., 2017).

Losanno et al. (2014) introduced the frequency response analysis for the isolation system of a bridge and proposed a simple procedure to determine the optimal value of the viscous coefficient or the yield displacement of the isolators. In the reference (Losanno et al., 2015), a design optimization problem was investigated for a simple linear-elastic one-bay, one-story frame equipped with elastic-deformable viscous or friction dissipative braces. An analytical approach was proposed for determining the theoretical optimal value of the viscous damping or the yielding force parameter, able to minimize the maximum displacements. Losanno et al. (2017) presented a numerical investigation on the seismic behavior of isolated bridges with supplemental viscous damping under both far field and near fault ground motions for both simply supported and continuous bridges. They demonstrated that the base isolation with the optimal damping is effective for reducing the displacement in the base-isolation story in bridges. It appears that the introduction of the optimization concept

https://doi.org/10.1016/j.heliyon.2019.e01221

in the design of supplemental damping in bridges and structures is important from the viewpoint of effectiveness in the response mitigation and robustness for a broad class of input (far-field and near-fault motions). A recent review on damper optimization was provided by Domenico et al. (2019).

In this paper, the multi impulse is introduced as a substitute for long-duration ground motions and a closed-form solution is derived for the critical steady-state response of an elastic perfectly-plastic SDOF model with nonlinear viscous damping under the multi impulse. Base-isolated building structures consisting of laminated natural rubber bearings, steel dampers and oil dampers with relief mechanism are considered as the elastic-plastic SDOF model with nonlinear viscous damping. The restoring-force characteristics of laminated natural rubber bearings and steel dampers are modeled by the elastic perfectly-plastic restoring force-deformation relation and the oil damper is modeled by the nonlinear viscous damping with relief mechanism. Oil dampers are being adopted for many building structures so that the maximum response under earthquake ground motions or wind loads is decreased and the vibrations are damped at an early stage. The oil damper has a damping mechanism to generate a damping force, proportional to the relative velocity of the piston, through the fluid resistance of inner oil and the damping valve (Tsuji et al., 2012). The damping force provided by the oil damper acts as an external load to braces or beam-column joints to which the oil dampers are mounted, and the mounting members or the beam-column joints to the oil dampers are possibly damaged when the damping force becomes excessively large. Therefore, the oil damper has the mechanism to prevent the increase of damping force by opening the relief valve when the damping force becomes larger than a specific value. This mechanism is called the relief mechanism and the damping force at the timing when the relief valve opens is called the relief force.

It may be difficult to derive an exact steady-state response of the SDOF elastic perfectly-plastic system with nonlinear viscous damping under the critical multi impulse by solving the differential equation directly, even by using the impulse input. Therefore, the steady-state response is derived approximately by using the energy balance law and the quadratic or elliptical approximation of the damping force-deformation relation following the previous approaches (Kojima et al., 2017; Hayashi et al., 2018). The multi impulse is introduced in Section 2.1. An SDOF elastic-perfectly plastic system with nonlinear viscous damping is introduced in Section 2.2. The critical timing of the multi impulse is investigated and six cases are introduced in the derivation of the critical responses under the multi impulse in Section 3.1. The energy approach and the approximation method of the damping force-deformation relation are also introduced in Section 3.1. A closed-form solution for the critical response under the multi impulse is derived approximately in Section 4.1. The accuracy of the approximate closed-form solution is investigated by the time-history response analysis to the multi impulse in Section 5.1. The validity of using

https://doi.org/10.1016/j.heliyon.2019.e01221

the multiple impulse as substitute for the long-period and long-duration ground motions is investigated through the comparison with the elastic-plastic response under the corresponding multi-cycle sine wave in Section 5.2. The reliability of the multi impulse as a substitute for the long-duration ground motions is also checked through the comparison with the elastic-plastic response under the recorded long-duration ground motion in Section 5.3. It is also shown that the nonlinearity in viscous damping causes a remarkable influence on the earthquake response in some cases. The conclusions are summarized at the end.

2. Model

2.1. Multi impulse as substitute for long-duration ground motions

Kojima and Takewaki (2015c, 2017) expressed the multi-cycle sine wave representing the principal part of long-duration ground motions in terms of the multi impulse. The multi impulse with constant time interval t_0, as shown in Fig. 1, is expressed by

$$\begin{aligned}\ddot{u}_g(t) =& V\delta(t) - V\delta(t-t_0) + V\delta(t-2t_0) - V\delta(t-3t_0) + \cdots + (-1)^{N-1} \\ & V\delta\{t-(N-1)t_0\},\end{aligned} \tag{1}$$

where V is the velocity imparted to masses or a mass by each impulse (the input velocity level), N is the number of impulses taken from the multi impulse and $\delta(t)$ is the Dirac delta function. The ground acceleration and velocity of the multi impulse and the corresponding multi-cycle sine wave, which represents a long-duration ground motion (Takewaki and Tsujimoto, 2011), are shown in Fig. 1 (V_l denotes the velocity amplitude of the multi-cycle sine wave with the period of T_l and will be explained later). It can be confirmed that the multi impulse is a better approximate of the corresponding sine wave in the form of velocity compared to the acceleration. In comparing the response under the multi impulse with that under the multi-cycle sine wave, it is essential to modulate the input level of two inputs. The input levels of the multi impulse and the multi-cycle sine wave are modulated by matching the maximum Fourier amplitude. The modulating method can be found in the reference (Kojima and Takewaki, 2015c, 2017).

For reference, the Fourier transform of $\ddot{u}_g(t)$ in Eq. (1) can be derived as shown in Eq. (2).

$$\begin{aligned}\ddot{U}_g(\omega) =& \int_{-\infty}^{\infty} \left[V\delta(t) - V\delta(t-t_0) + \cdots + (-1)^{N-1} V\delta\{t-(N-1)t_0\}\right] e^{-i\omega t} dt \\ =& V\sum\nolimits_{n=0}^{N-1} (-1)^n e^{-i\omega n t_0}\end{aligned} \tag{2}$$

https://doi.org/10.1016/j.heliyon.2019.e01221

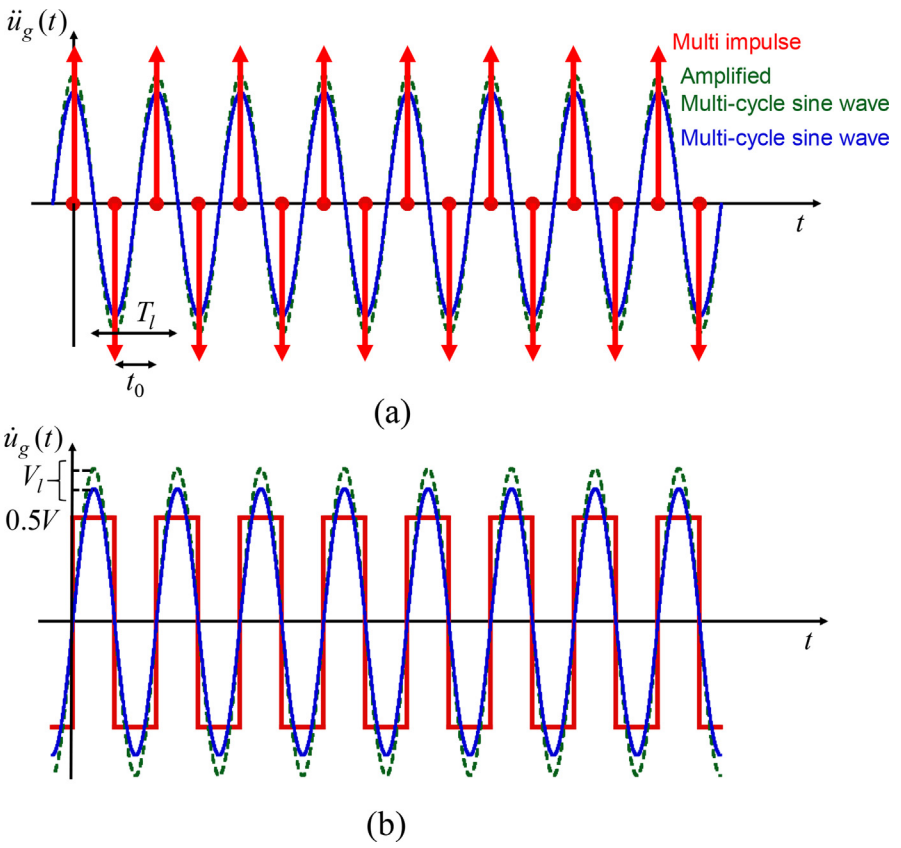

Fig. 1. Multi impulse, sine wave and amplified sine wave, (a) Acceleration, (b) Velocity.

2.2. Elastic perfectly-plastic SDOF model with nonlinear viscous damping

Consider an elastic perfectly-plastic SDOF model, as shown in Fig. 2, with nonlinear viscous damping. This model has mass m, stiffness k and damping coefficient c. The damping coefficient is constant regardless of yielding. Let $\omega_1 = \sqrt{k/m}$, $T_1 = 2\pi/\omega_1$ and $h = c/(2\sqrt{km})$ denote the undamped natural circular frequency, the undamped natural period and the damping ratio, respectively. Furthermore, let$\omega'_1 = \sqrt{1-h^2}\omega_1$ and $T'_1 = 2\pi/\omega'_1$ denote the damped natural circular frequency and the damped natural period, respectively. The parameters u, f_R and f_D are the displacement of the mass relative to the ground (deformation of the system), the restoring force and damping force of the system, respectively, and the parameters d_y and $f_y = kd_y$ are the yield deformation and the yield force. The oil damper with relief mechanism is treated as a nonlinear viscous damper. V_{DR} denotes the relief velocity and the damping force is constant at the relief force $f_{DR} = cV_{DR}$ after the velocity becomes larger than V_{DR}.

https://doi.org/10.1016/j.heliyon.2019.e01221

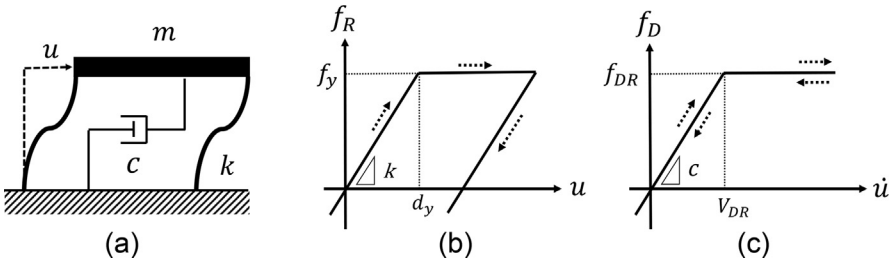

Fig. 2. Elastic perfectly-plastic SDOF model with nonlinear viscous damping, (a) SDOF model, (b) Restoring force-deformation relation, (c) Damping force-velocity relation.

V_y obtained by the following equation (Eq. (3)) denotes the input level of the single impulse at which the SDOF model just attains the yield deformation after single impulse.

$$\frac{1}{2}mV_y^2 = \frac{1}{2}kd_y^2 \Leftrightarrow V_y = \omega_1 d_y \tag{3}$$

This parameter also presents a strength parameter with velocity dimension. In the following sections, the deformation of the model is normalized by d_y and the input velocity is normalized by V_y. The normalized values are denoted by an over-bar.

3. Theory

3.1. Maximum response of elastic perfectly-plastic SDOF model with nonlinear viscous damping under critical multi impulse

The critical timing of each impulse, which maximizes the plastic deformation amplitude u_p, is investigated for the elastic perfectly-plastic SDOF model with nonlinear viscous damping. Fig. 3 shows the transition of the critical time interval t_0/T_1, normalized by the natural period, with respect to the normalized input velocity level V/V_y for $V_{DR}/V_y = 0.5, 1.5, 2.5$ and $h = 0.15, 0.30$. From Fig. 3, it can be observed that the critical timing t_0 of each impulse is the timing such that each impulse acts at the state corresponding to the zero restoring-force (called 'the zero restoring-force timing') in the lower input velocity level and it shifts from the zero restoring-force timing to the timing such that each impulse acts at the state corresponding to the maximum velocity of the mass (called 'the maximum velocity timing') as the input velocity becomes larger. This is because the damping force remains the relief force in larger input levels.

The zero restoring-force timing and the maximum velocity timing are assumed as the critical timing of each impulse and the closed-form plastic deformation amplitude u_p is approximately derived for the elastic perfectly-plastic model with nonlinear viscous damping under the critical multi impulse in the following section. Then two solutions for u_p can be derived under the multi impulse such that each impulse acts at the zero

https://doi.org/10.1016/j.heliyon.2019.e01221

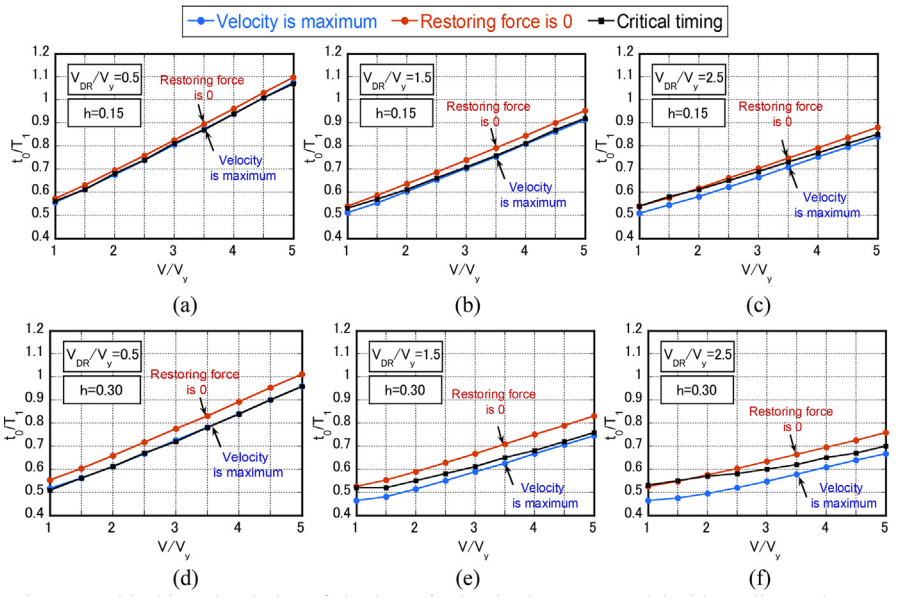

Fig. 3. Critical impulse timing of elastic perfectly-plastic SDOF model with nonlinear viscous damping under multi impulse, (a) $h = 0.15$, $V_{DR}/V_y = 0.5$, (b) $h = 0.15$, $V_{DR}/V_y = 1.5$, (c) $h = 0.15$, $V_{DR}/V_y = 2.5$, (d) $h = 0.30$, $V_{DR}/V_y = 0.5$, (e) $h = 0.30$, $V_{DR}/V_y = 1.5$, (f) $h = 0.30$, $V_{DR}/V_y = 2.5$.

restoring-force timing or at the maximum velocity timing. The larger one in u_p is adopted as the true plastic deformation amplitude under the critical multi impulse.

3.2. Maximum response under critical multi impulse

The critical steady-state response can be classified by the existence range of the restoring force and the damping force.

The steady state with plastic deformation is only treated in this paper. The schematic diagram of the point-symmetric restoring force-deformation relation in the steady state is shown in Fig. 4. Let $u_p, u_{\max 1}, u_{\max 2}$ denote the plastic deformation amplitude, the negative maximum deformation (absolute value) and the positive maximum deformation in the steady state. The quantity u_m is the deformation difference between the zero restoring-force point and the maximum velocity point. A residual deformation sometimes exists and changes depending on the input level of the impulse. It should be noted that the plastic deformation amplitude is not affected by value of the residual deformation.

The critical steady-state response can be classified into three cases in terms of the damping force depending on the input velocity level. CASE M1 is the case where the damping force does not attain the relief force. CASE M2 is the case where the damping force just before each impulse does not attain the relief force but the damping force just after each impulse attains the relief force. Furthermore, CASE M3 is

https://doi.org/10.1016/j.heliyon.2019.e01221

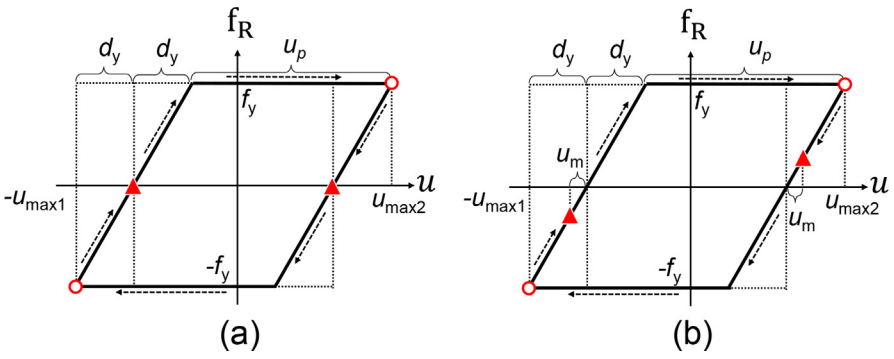

Fig. 4. Restoring force-deformation relation (circle/maximum response, triangle/acting point of impulse), (a) Impulse timing: Restoring force is zero, (b) Impulse timing: Velocity is maximum.

the case where the damping force attains the relief force before impulse. Fig. 5 shows the schematic diagram of the damping force-deformation relation in the steady-state response under the critical multi impulse in the case where the impulse timing is the zero restoring force timing. On the other hand, Fig. 6 shows the similar one in the case where the impulse timing is the maximum velocity timing. It should be noted that the difference in Figs. 5 and 6 can be seen only in the deformation axis because the force axis in Fig. 4 for characterizing the zero restoring-force timing is f_R and the force axis in Figs. 5 and 6 is f_D.

The closed-form solutions for the steady-state response in above three cases are derived under the multi impulse in which each impulse acts at the zero restoring-force timing or the maximum velocity timing in the following section.

3.3. Energy equivalent method and approximation in damping force-deformation relation

Hayashi et al. (2018) have derived the approximate closed-form expression of the plastic deformation amplitude of the elastic-perfectly plastic system with linear viscous damping under the critical multiple impulse. The plastic deformation

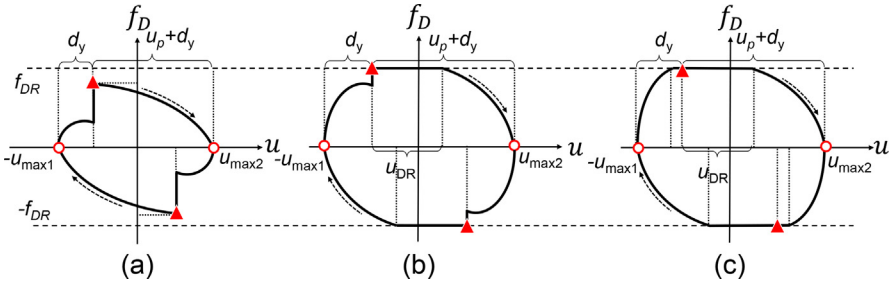

Fig. 5. Damping force-deformation relation (circle/maximum response, triangle/acting point of impulse) (Impulse timing: Restoring force is zero), (a) CASE M1, (b) CASE M2, (c) CASE M3.

https://doi.org/10.1016/j.heliyon.2019.e01221

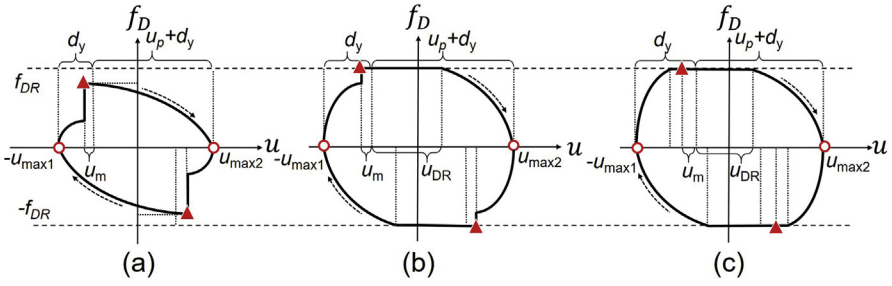

Fig. 6. Damping force-deformation relation (circle/maximum response, triangle/acting point of impulse) (Impulse timing: Velocity is maximum), (a) CASE M1, (b) CASE M2, (c) CASE M3.

amplitude under the critical multiple impulse can be derived by using an energy balance law without solving directly the equation of motion (differential equation). In the elastic-plastic system with viscous damping, the kinetic energy given at time of each impulse is transformed into the sum of the elastic strain energy corresponding to the yield deformation, the energy dissipated during the plastic deformation and the work done by the damping force (the energy dissipated by the viscous damping). In order to obtain the plastic deformation by the energy balance law, it is necessary that the damping force-deformation relation is approximated by the simple function. In the previous papers by Kojima et al. (2017) and Hayashi et al. (2018), the quadratic function has been used to approximate the damping force-deformation relation.

In the derivation of the plastic deformation amplitude in the following section, the curved portion in the damping force-deformation relation is approximated by the quadratic or elliptical function appropriately. Figs. 7 and 8 show the approximation method of the damping force-deformation relation by the quadratic and elliptical functions. The dashed areas in red indicates the energy by the approximate curve and the dashed area in grey means the energy by the exact curve. The quantities u'_{DR1}, u'_m, v'_m are defined in Section '**Closed-form solution (Impulse timing: Zero restoring-force timing)**'.

4. Method

4.1. Non-iterative determination of plastic deformation of model with nonlinear viscous damping under critical multi impulse

An approximate closed-form solution is derived for the plastic deformation amplitude of the elastic perfectly-plastic model with nonlinear viscous damping under the critical multi impulse. First, the plastic deformation amplitude under the multi impulse is derived in Section 4.2 under the assumption that each impulse acts at the zero restoring-force timing. Then, it is derived in Section 4.3 under the assumption that each impulse acts at the maximum velocity timing.

https://doi.org/10.1016/j.heliyon.2019.e01221

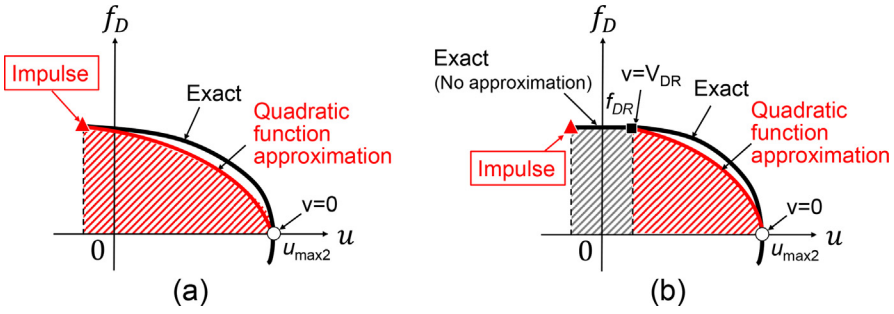

Fig. 7. Quadratic approximation of damping force-deformation relation, (a) CASE M1, (b) CASE M2, M3.

4.2. Closed-form solution (Impulse timing: Zero restoring-force timing)

(i) CASE M1

CASE M1 is the case where the damping force does not attain the relief force. Let v_c denote the velocity at the zero restoring-force timing, and v_c can be obtained by solving the following equation.

$$\begin{cases} m\ddot{u} + c\dot{u} + ku + k(u_{\max 1} - d_y) = 0 \\ u(0) = -u_{\max 1} \ , \ \dot{u}(0) = 0 \ , \ u(t_c) = -u_{\max 1} + d_y \ , \ \dot{u}(t_c) = v_c \end{cases}, \tag{4}$$

where $t_c = \{0.5\pi + \arctan(h/\sqrt{1-h^2})\}/\omega'_1$ is the time interval between the maximum deformation point and the zero restoring-force point. From Eq. (4), the normalized velocity $\overline{v}_c (= v_c/V_y)$ at the zero restoring-force timing can be obtained by

$$\overline{v}_c = \exp\left\{ -\frac{h}{\sqrt{1-h^2}}\left(\frac{\pi}{2} + \arctan\frac{h}{\sqrt{1-h^2}}\right)\right\} = a_c. \tag{5}$$

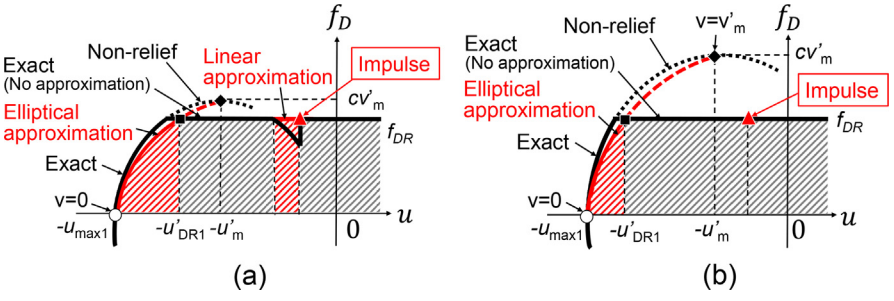

Fig. 8. Elliptical approximation of damping force-deformation relation, (a) Damping force is not beyond relief force when restoring force is 0, (b) Damping force is beyond relief force when restoring force is 0.

https://doi.org/10.1016/j.heliyon.2019.e01221

The damping force-deformation relation is approximated by a quadratic function with the vertex $(u,f_D) = (u_{\max 2}, 0)$ and passing the point $(u,f_D) = (u_{\max 2} - u_p - d_y, cV + cv_c)$. The damping force f_D can be obtained as follows (see Figs. 5(a) and 7(a)).

$$f_D = c(v_c + V)\sqrt{\frac{u_{\max 2} - u}{u_p + d_y}} \tag{6}$$

The work by the damping force for deformation can be obtained by integrating Eq. (6) from $u = u_{\max 2} - u_p - d_y$ to $u = u_{\max 2}$.

$$E_D = \int_{u_{\max 2} - u_p - d_y}^{u_{\max 2}} f_D du = \frac{2}{3} c(V + v_c)\left(u_p + d_y\right) \tag{7}$$

The energy balance law between the impulse acting point (the zero restoring-force timing) and the point attaining the maximum deformation can be expressed as follows.

$$\frac{1}{2} m(V + v_c)^2 = \frac{1}{2} k d_y^2 + k d_y u_p + E_D \tag{8}$$

From Eqs. (7) and (8), the normalized plastic deformation amplitude $\overline{u}_p (= u_p / d_y)$ can be expressed by Eq. (9).

$$\overline{u}_p = \frac{3\left(\overline{V} + \overline{v}_c\right)^2 - 3 - 8h\left(\overline{V} + \overline{v}_c\right)}{2\left\{3 + 4h\left(\overline{V} + \overline{v}_c\right)\right\}} \tag{9}$$

(ii) CASE M2

CASE M2 is the case where the damping force attains the relief force only just after each impulse. The velocity v_c at the zero restoring-force timing can be obtained by Eq. (5) as in CASE M1. The curved part in the damping force-deformation relation is approximated by a quadratic function as shown in Figs. 5(b) and 7(b), and the work by the damping force from the impulse acting point to the maximum deformation can be obtained approximately.

u_{DR} is the displacement from the impulse acting point to the point where the damping force just becomes smaller than the relief force as shown in Fig. 5(b). If $u_{DR} < d_y$, u_{DR} can be derived as

$$\frac{1}{2} m(v_c + V)^2 = \frac{1}{2} m V_{DR}^2 + \frac{1}{2} k u_{DR}^2 + c V_{DR} u_{DR} \tag{10}$$

https://doi.org/10.1016/j.heliyon.2019.e01221

$$\Leftrightarrow \overline{u}_{DR} = \sqrt{\left(\overline{v}_c + \overline{V}\right)^2 + (4h^2 - 1)\overline{V}_{DR}^2} - 2h\overline{V}_{DR} \tag{11}$$

On the other hand, if $d_y < u_{DR}$, u_{DR} can be obtained as

$$\frac{1}{2}m(v_c + V)^2 = \frac{1}{2}mV_{DR}^2 + \frac{1}{2}kd_y^2 + kd_y\left(u_{DR} - d_y\right) + cV_{DR}u_{DR} \tag{12}$$

$$\Leftrightarrow \overline{u}_{DR} = \frac{\left(\overline{v}_c + \overline{V}\right)^2 - \overline{V}_{DR}^2 + 1}{2\left(1 + 2h\overline{V}_{DR}\right)} \tag{13}$$

When $u_{DR} = d_y$, $\overline{u}_{DR}$ derived by Eq. (11) is equal to that derived by Eq. (13). The boundary input velocity level between Eqs. (11) and (13) is denoted by V_{bc}. From Eq. (10) or (12) and $u_{DR} = d_y$, the boundary input velocity level $\overline{V}_{bc} = (V_{bc}/V_y)$ can be obtained by Eq. (14).

$$\overline{V}_{bc} = \sqrt{1 + 4h\overline{V}_{DR} + \overline{V}_{DR}^2} - \overline{v}_c. \tag{14}$$

The curved part in the damping force−deformation relation is approximated by a quadratic function with the vertex $(u, f_D) = (u_{\max 2}, 0)$ and passing the point $(u, f_D) = \left(u_{\max 2} - u_p - d_y + u_{DR}, cV_{DR}\right)$. The damping force f_D can be obtained as follows (Figs. 5(b) and 7(b)).

$$f_D = cV_{DR}\sqrt{\frac{u_{\max 2} - u}{\left(u_p + d_y\right) - u_{DR}}} \tag{15}$$

By integrating Eq. (15) from $u = u_{\max 2} - u_p - d_y + u_{DR}$ to $u = u_{\max 2}$, the work by the damping force approximated by the quadratic function is obtained by

$$\int_{u_{\max 2} - u_p - d_y + u_{DR}}^{u_{\max 2}} cV_{DR}\sqrt{\frac{u_{\max 2} - u}{\left(u_p + d_y\right) - u_{DR}}}du = \frac{2}{3}cV_{DR}\left(u_p + d_y - u_{DR}\right) \tag{16}$$

From Eq. (16) and the work by the relief force from $u = u_{\max 2} - u_p - d_y$ to $u = u_{\max 2} - u_p - d_y + u_{DR}$, the work by the damping force from $u = u_{\max 2} - u_p - d_y$ to $u = u_{\max 2}$ can be obtained as follows.

$$E_D = cV_{DR}u_{DR} + \frac{2}{3}cV_{DR}\left(u_p + d_y - u_{DR}\right) = \frac{1}{3}cV_{DR}\left(2u_p + 2d_y + u_{DR}\right) \tag{17}$$

The energy balance law between the impulse acting point and the point attaining the maximum deformation can be expressed as follows.

https://doi.org/10.1016/j.heliyon.2019.e01221

$$\frac{1}{2}m(v_c+V)^2=\frac{1}{2}kd_y^2+kd_yu_p+E_D \tag{18}$$

From Eqs. (17) and (18), the plastic deformation amplitude u_p can be obtained by

$$\overline{u}_p=\frac{3\left(\overline{v}_c+\overline{V}\right)^2-3-4h\overline{V}_{DR}(\overline{u}_{DR}+2)}{2\left(3+4h\overline{V}_{DR}\right)}. \tag{19}$$

From Eqs. (11), (13), and (19), the plastic deformation u_p can be expressed by

$$\overline{u}_p=\begin{cases}\dfrac{3\left(\overline{v}_c+\overline{V}\right)^2-3+8h\overline{V}_{DR}\left(h\overline{V}_{DR}-1\right)}{2\left(3+4h\overline{V}_{DR}\right)}-\dfrac{2h\overline{V}_{DR}}{3+4h\overline{V}_{DR}}\sqrt{\left(\overline{v}_c+\overline{V}\right)^2+\left(4h^2-1\right)\overline{V}_{DR}^2} & \left(\overline{V}<\overline{V}_{bc}\right)\\ \dfrac{\left(\overline{v}_c+\overline{V}\right)^2}{2\left(1+2h\overline{V}_{DR}\right)}+\dfrac{2h\overline{V}_{DR}\left(\overline{V}_{DR}^2-8h\overline{V}_{DR}-8\right)-3}{2\left(1+2h\overline{V}_{DR}\right)\left(3+4h\overline{V}_{DR}\right)} & \left(\overline{V}>\overline{V}_{bc}\right)\end{cases} \tag{20}$$

(iii) CASE M3

CASE M3 is the case where the damping force attains the relief force before impulse. In this case, if the velocity v_c at the zero restoring-force timing can be obtained, the plastic deformation amplitude u_p can be obtained by Eq. (20). Therefore, v_c in CASE M3 is derived here.

To obtain v_c, it is assumed that each impulse acts at the zero restoring-force timing in the elastic perfectly-plastic SDOF model with linear viscous damping. The deformation and velocity of the model with linear viscous damping at the point where the damping force is maximum are denoted by $-u'_m$ and v'_m, as shown in Fig. 8(b). u'_m and v'_m can be obtained by

$$\begin{cases}m\ddot{u}+c\dot{u}+ku+k\left(u_{\max 1}-d_y\right)=0\\ u(0)=-u_{\max 1}\ ,\ \ \dot{u}(0)=0\ ,\ \ u(t'_m)=-u'_m\ ,\ \ \dot{u}(t'_m)=v'_m\end{cases}, \tag{21}$$

where $t'_m=\{0.5\pi-\arctan(h/\sqrt{1-h^2}\,)\}/\omega'_1$ is the time interval between the maximum velocity point and the maximum deformation point in the model with liner viscous damping. From Eq. (21), $\overline{u}'_m\left(=u'_m/d_y\right)$ and $\overline{v}'_m\left(=v'_m/V_y\right)$ can be derived by Eqs. (22) and (23).

$$\overline{u}'_m=2h\overline{v}'_m+\left(u_{\max 1}-d_y\right)/d_y\,, \tag{22}$$

https://doi.org/10.1016/j.heliyon.2019.e01221

$$\overline{v}'_m = \exp\left\{ -\frac{h}{\sqrt{1-h^2}}\left(\frac{\pi}{2} - \arctan\frac{h}{\sqrt{1-h^2}}\right)\right\} = a_m, \tag{23}$$

The curved part in the damping force-deformation relation is approximated by an ellipse with the two vertexes $(-u'_m, cv'_m)$ and $(-u_{\max 1}, 0)$. The damping force f_D in the second quadrant ($f_D \geq 0, u \leq 0$) can be obtained from Eq. (24).

$$f_D = cv'_m\sqrt{1-\left(\frac{u+u'_m}{u_{\max 1}-u'_m}\right)^2} \tag{24}$$

The deformation at the point where the approximate ellipse and the line $f_D = cV_{DR}$ intersect is denoted by $-u'_{DR1}$. Then u'_{DR1} can be obtained by

$$\overline{u}'_{DR1} = 2ha_m + \frac{1-2ha_m}{a_m}\sqrt{a_m^2 - \overline{V}_{DR}^2} + (\overline{u}_{\max 1} - 1). \tag{25}$$

v_c can be derived by using u'_{DR1} and an energy balance law between the point $(-u'_{DR1}, cV_{DR})$ and the zero restoring force timing. Although it is possible that, regardless of the fact that the damping force attains the relief force, the damping force before the input of impulse is smaller than f_{DR} at the zero restoring-force point depending on the input velocity level, such decrease of the damping force is ignored here and the damping force between the point $(-u'_{DR1}, cV_{DR})$ and the zero restoring force point is approximated to be constant by the relief force here (Fig. 8(a)). The energy balance law between the point $(-u'_{DR1}, cV_{DR})$ and the zero restoring force timing can be expressed by

$$\frac{1}{2}mV_{DR}^2 + \frac{1}{2}k\left(u'_{DR1} - u_{\max 1} + d_y\right)^2 = \frac{1}{2}mv_c^2 + cV_{DR}\left(u'_{DR1} - u_{\max 1} + d_y\right). \tag{26}$$

From Eq. (26), the following equation can be obtained.

$$\overline{v}_c = \sqrt{\overline{V}_{DR}^2 + \left(\overline{u}'_{DR1} - \overline{u}_{\max 1} + 1\right)^2 - 4h\overline{V}_{DR}\left(\overline{u}'_{DR1} - \overline{u}_{\max 1} + 1\right)}. \tag{27}$$

From Eqs. (25) and (27), the velocity $\overline{v}_c (= v_c/V_y)$ at the zero restoring-force timing can be expressed by Eq. (28).

$$\overline{v}_c = \sqrt{\overline{V}_{DR}^2 - 8h^2a_m\overline{V}_{DR} + (2ha_m)^2 + \left(\frac{1-2ha_m}{a_m}\right)^2\left(a_m^2 - \overline{V}_{DR}^2\right) + \frac{4h(1-2ha_m)\left(a_m - \overline{V}_{DR}\right)}{a_m^2}\sqrt{a_m^2 - \overline{V}_{DR}^2}}. \tag{28}$$

https://doi.org/10.1016/j.heliyon.2019.e01221

4.3. Closed-form solution (Impulse timing: Maximum velocity timing)

The plastic deformation amplitude u_p is derived here for the elastic perfectly-plastic model with nonlinear viscous damping under the multi impulse in the case where each impulse acts at the maximum velocity timing.

(i) CASE M1

CASE M1 is the case where the damping force does not attain the relief force. Let v_m denote the velocity at the maximum velocity timing after each impulse. The displacement at the maximum velocity point from the zero restoring-force point is denoted by u_m. v_m and u_m can be obtained from Eq. (29) by solving equation of motion.

$$\begin{cases} m\ddot{u}+c\dot{u}+ku+k\left(u_{\max 1}-d_y\right)=0 \\ u(0)=-u_{\max 1}\ ,\ \ \dot{u}(0)=0\ ,\ u(t_m)=-u_m-\left(u_{\max 1}-d_y\right)\ ,\ \ \dot{u}(t_m)=v_m\ , \\ \ddot{u}(t_m)=0 \end{cases} \tag{29}$$

$$\overline{u}_m=2h\overline{v}_m \tag{30}$$

$$\overline{v}_m=\exp\left\{-\frac{h}{\sqrt{1-h^2}}\left(\frac{\pi}{2}-\arctan\frac{h}{\sqrt{1-h^2}}\right)\right\}=a_m, \tag{31}$$

where $t_m=\{0.5\pi-\arctan(h/\sqrt{1-h^2})\}/\omega'_1$ is the time interval between the maximum velocity point and the maximum deformation point. The damping force−deformation relation is approximated by a quadratic function with the vertex $(u,f_D)=(u_{\max 2},0)$ and passing the point $(u,f_D)=(u_{\max 2}-u_p-d_y-u_m,cV+cv_m)$. The damping force f_D can be obtained as follows (see Figs. 6(a) and 7(a)).

$$f_D=c(v_m+V)\sqrt{\frac{u_{\max 2}-u}{u_p+d_y+u_m}} \tag{32}$$

The work by the damping force can be obtained as follows by integrating Eq. (32) from $u=u_{\max 2}-u_p-d_y-u_m$ to $u=u_{\max 2}$.

$$E_D=\int_{u_{\max 2}-u_p-d_y-u_m}^{u_{\max 2}} f_D du=\frac{2}{3}c(V+v_m)\left(u_p+d_y+u_m\right) \tag{33}$$

The energy balance law between the impulse acting point (the maximum velocity timing) and the point attaining the maximum deformation can be expressed as follows.

$$\frac{1}{2}m(V+v_m)^2+\frac{1}{2}ku_m^2=\frac{1}{2}kd_y^2+kd_yu_p+E_D \tag{34}$$

https://doi.org/10.1016/j.heliyon.2019.e01221

From Eqs. (30), (31), (33), and (34), the normalized plastic deformation amplitude $\overline{u}_p(=u_p/d_y)$ can be expressed by Eq. (35):

$$\overline{u}_p = \frac{3\left(\overline{V}+\overline{v}_m\right)^2 - 3 - 8h\left(\overline{V}+\overline{v}_m\right) - 4h^2\overline{v}_m\left(4\overline{V}+\overline{v}_m\right)}{2\left\{3+4h\left(\overline{V}+\overline{v}_m\right)\right\}} \tag{35}$$

(ii) CASE M2

CASE M2 is the case where the damping force attains the relief force only after each impulse. The velocity v_m at the impulse acting point is obtained by Eq. (31) as in CASE M1.

The curved part in the damping force-deformation relation is approximated by a quadratic function as shown in Figs. 6(b) and 7(b), and the work by the damping force from the impulse acting point to the maximum deformation can be obtained. The displacement from the impulse acting point to the point where the damping force just becomes smaller than the relief force is denoted by $u_{DR}+u_m$ as shown in Fig. 6(b), and u_{DR} can be obtained by the energy balance law. If $u_{DR} < d_y$, u_{DR}can be obtained as

$$\frac{1}{2}m(v_m+V)^2 + \frac{1}{2}ku_m^2 = \frac{1}{2}mV_{DR}^2 + \frac{1}{2}ku_{DR}^2 + cV_{DR}(u_m+u_{DR}) \tag{36}$$

$$\Leftrightarrow \overline{u}_{DR} = -2h\overline{V}_{DR} + \sqrt{\left(\overline{v}_m+\overline{V}\right)^2 + (4h^2-1)\overline{V}_{DR}^2 + \overline{u}_m\left(\overline{u}_m - 4h\overline{V}_{DR}\right)} \tag{37}$$

On the other hand, if $d_y < u_{DR}$, u_{DR} can be derived as

$$\frac{1}{2}m(v_m+V)^2 + \frac{1}{2}ku_m^2 = \frac{1}{2}mV_{DR}^2 + \frac{1}{2}kd_y^2 + kd_y\left(u_{DR}-d_y\right) + cV_{DR}(u_m+u_{DR}) \tag{38}$$

$$\Leftrightarrow \overline{u}_{DR} = \frac{\left(\overline{v}_m+\overline{V}\right)^2 - \overline{V}_{DR}^2 + 1 + \overline{u}_m\left(\overline{u}_m - 4h\overline{V}_{DR}\right)}{2\left(1+2h\overline{V}_{DR}\right)} \tag{39}$$

When $u_{DR} = d_y$, $\overline{u}_{DR}$ derived by Eq. (37) is equal to that derived by Eq. (39). From Eq. (36) or (38) and $u_{DR} = d_y$, the boundary input velocity level $\overline{V}_{bm}(=V_{bm}/V_y)$ can be obtained by

$$\overline{V}_{bm} = \sqrt{\overline{V}_{DR}^2 + 4h\overline{V}_{DR} + 1 - \overline{u}_m\left(\overline{u}_m - 4h\overline{V}_{DR}\right)} - \overline{v}_m. \tag{40}$$

From Eqs. (30), (31), (37), (39), and (40), $\overline{u}_{DR}(=u_{DR}/d_y)$ can be expressed by Eqs. (41) and (42).

https://doi.org/10.1016/j.heliyon.2019.e01221

$$\overline{u}_{DR}=\begin{cases}\sqrt{\left(\overline{v}_m+\overline{V}\right)^2+\left(4h^2-1\right)\overline{V}_{DR}^2+4h^2\overline{v}_m\left(\overline{v}_m-2\overline{V}_{DR}\right)}-2h\overline{V}_{DR} & \left(\overline{V}<\overline{V}_{bm}^{(\mathrm{M2})}\right)\\ \dfrac{\left(\overline{v}_m+\overline{V}\right)^2-\overline{V}_{DR}^2+1+4h^2\overline{v}_m\left(\overline{v}_m-2\overline{V}_{DR}\right)}{2\left(1+2h\overline{V}_{DR}\right)} & \left(\overline{V}>\overline{V}_{bm}^{(\mathrm{M2})}\right)\end{cases} \tag{41}$$

$$\overline{V}_{bm}^{(\mathrm{M2})}=\sqrt{\overline{V}_{DR}^2+4h\overline{V}_{DR}+1-4h^2\overline{v}_m\left(\overline{v}_m-2\overline{V}_{DR}\right)}-a_m, \tag{42}$$

where $V_{bm}^{(\mathrm{M2})}$ denotes the boundary input velocity level between Eqs. (37) and (39) in CASE M2.

The curved part in the damping force−deformation relation is also approximated by Eq. (15) and the work by the damping force from $u=u_{\max 2}-u_p-d_y$ to $u=u_{\max 2}$ can be expressed as follows (Figs. 6(b) and 7(b)).

$$E_D=cV_{DR}(u_{DR}+u_m)+\frac{2}{3}cV_{DR}\left(u_p+d_y-u_{DR}\right)=\frac{1}{3}cV_{DR}\left(u_{DR}+3u_m+2u_p+2d_y\right) \tag{43}$$

The energy balance law between the impulse acting point and the point attaining the maximum deformation can be expressed as

$$\frac{1}{2}m(v_m+V)^2+\frac{1}{2}ku_m^2=\frac{1}{2}kd_y^2+kd_yu_p+E_D \tag{44}$$

From Eqs. (43) and (44), the plastic deformation amplitude u_p can be obtained by

$$\overline{u}_p=\frac{3\left(\overline{v}_m+\overline{V}\right)^2-3-8h\overline{V}_{DR}+3\overline{u}_m\left(\overline{u}_m-4h\overline{V}_{DR}\right)-4h\overline{V}_{DR}\overline{u}_{DR}}{2\left(3+4h\overline{V}_{DR}\right)} \tag{45}$$

From Eqs. (30), (31), (41), and (45), the plastic deformation amplitude $\overline{u}_p(=u_p/d_y)$ can be obtained as Eq. (46).

$$\overline{u}_p=\begin{cases}\dfrac{3\left(\overline{v}_m+\overline{V}\right)^2+12h^2\overline{v}_m\left(\overline{v}_m-2\overline{V}_{DR}\right)-3+8h\overline{V}_{DR}\left(h\overline{V}_{DR}-1\right)}{2\left(3+4h\overline{V}_{DR}\right)} & \left(\overline{V}<\overline{V}_{bm}^{(\mathrm{M2})}\right)\\ -\dfrac{2h\overline{V}_{DR}}{3+4h\overline{V}_{DR}}\sqrt{\left(\overline{v}_m+\overline{V}\right)^2+\left(4h^2-1\right)\overline{V}_{DR}^2+4h^2\overline{v}_{\mathrm{m}}\left(\overline{v}_{\mathrm{m}}-2\overline{V}_{DR}\right)} & \\ \dfrac{\left(\overline{v}_m+\overline{V}\right)^2+4h^2\overline{v}_m\left(\overline{v}_m-2\overline{V}_{DR}\right)}{2\left(1+2h\overline{V}_{DR}\right)}+\dfrac{2h\overline{V}_{DR}\left(\overline{V}_{DR}^2-8h\overline{V}_{DR}-8\right)-3}{2\left(1+2h\overline{V}_{DR}\right)\left(3+4h\overline{V}_{DR}\right)} & \left(\overline{V}>\overline{V}_{bm}^{(\mathrm{M2})}\right)\end{cases} \tag{46}$$

https://doi.org/10.1016/j.heliyon.2019.e01221

(iii) CASE M3

CASE M3 is the case where the damping force attains the relief force before impulse. The velocity v_m at the impulse acting timing can be obtained by approximating the curved part in the damping force-deformation relation with an ellipse. The displacement $-u'_{DR1}$ at the point where the approximate ellipse and the line $f_D = cV_{DR}$ intersect can be obtained by Eq. (25). The displacement of the point where the velocity is maximum from the zero restoring-force point is denoted by u_m as shown in Figs. 6(c) and 8(b). v_m and u_m can be obtained from Eq. (47) by solving equation of motion.

$$\begin{cases} m\ddot{u} + cV_{DR} + ku + k\left(u_{\max 1} - d_y\right) = 0 \\ u(0) = -u'_{DR1}\ ,\ \ \dot{u}(0) = V_{DR}\ ,\ u(t_m) = -u_m - \left(u_{\max 1} - d_y\right)\ ,\ \dot{u}(t_m) = v_m\ , \\ \ddot{u}(t_m) = 0 \end{cases} \tag{47}$$

$$\overline{u}_m = 2h\overline{V}_{DR} \tag{48}$$

$$\overline{v}_m = \sqrt{\left\{\overline{u}'_{DR1} - 2h\overline{V}_{DR} - (\overline{u}_{\max 1} - 1)\right\}^2 + \overline{V}_{DR}^2}, \tag{49}$$

By substituting $-u'_{DR1}$ given in Eq. (25) into Eq. (49), the following equation, Eq. (50), can be obtained.

$$\overline{v}_m = \sqrt{\left\{2h\left(a_m - \overline{V}_{DR}\right) + \frac{1 - 2ha_m}{a_m}\sqrt{a_m^2 - \overline{V}_{DR}^2}\right\}^2 + \overline{V}_{DR}^2} \tag{50}$$

By substituting $\overline{u}_m (= u_m/d_y)$ given by Eq. (48) into Eqs. (37), (39), and (40), $\overline{u}_{DR} (= u_{DR}/d_y)$ and the boundary input velocity level $\overline{V}_{bm}^{(\mathrm{M3})} \left(= V_{bm}^{(\mathrm{M3})}/V_y\right)$ of u_{DR} in CASE M3 can be obtained by Eqs. (51) and (52).

$$\overline{u}_{DR} = \begin{cases} \sqrt{\left(\overline{v}_m + \overline{V}\right)^2 - \overline{V}_{DR}^2} - 2h\overline{V}_{DR} & \left(\overline{V} < \overline{V}_{bm}^{(\mathrm{M3})}\right) \\ \dfrac{\left(\overline{v}_m + \overline{V}\right)^2 - \left(4h^2 + 1\right)\overline{V}_{DR}^2 + 1}{2\left(1 + 2h\overline{V}_{DR}\right)} & \left(\overline{V} > \overline{V}_{bm}^{(\mathrm{M3})}\right) \end{cases} \tag{51}$$

$$\begin{aligned} \overline{V}_{bm}^{(\mathrm{M3})} = {} & \sqrt{(4h^2 + 1)\overline{V}_{DR}^2 + 4h\overline{V}_{DR} + 1} \\ & - \sqrt{\left\{2h\left(a_m - \overline{V}_{DR}\right) + \frac{1 - 2ha_m}{a_m}\sqrt{a_m^2 - \overline{V}_{DR}^2}\right\}^2 + \overline{V}_{DR}^2} \end{aligned} \tag{52}$$

The plastic deformation amplitude u_p can be expressed by Eq. (45) as in CASE M2. By substituting $\overline{u}_m \left(= u_m/d_y\right)$, $\overline{v}_m (= v_m/V_y)$ and $\overline{u}_{DR} (= u_{DR}/d_y)$ obtained by Eqs. (48), (49), and (51) into Eq. (45), u_p in CASE M3 can be obtained as Eq. (53).

https://doi.org/10.1016/j.heliyon.2019.e01221

$$\overline{u}_p = \begin{cases} \dfrac{3\left(\overline{v}_m + \overline{V}\right)^2 - 3 - 4h\overline{V}_{DR}\left(h\overline{V}_{DR} + 2\right)}{2\left(3 + 4h\overline{V}_{DR}\right)} - \dfrac{2h\overline{V}_{DR}}{3 + 4h\overline{V}_{DR}}\sqrt{\left(\overline{v}_m + \overline{V}\right)^2 - \overline{V}_{DR}^2} & \left(\overline{V} < \overline{V}_{bm}^{(\mathrm{M3})}\right) \\ \dfrac{\left(\overline{v}_m + \overline{V}\right)^2 - 4h^2\overline{V}_{DR}^2}{2\left(1 + 2h\overline{V}_{DR}\right)} + \dfrac{2h\overline{V}_{DR}\left(\overline{V}_{DR}^2 - 8h\overline{V}_{DR} - 8\right) - 3}{2\left(1 + 2h\overline{V}_{DR}\right)\left(3 + 4h\overline{V}_{DR}\right)} & \left(\overline{V} > \overline{V}_{bm}^{(\mathrm{M3})}\right) \end{cases} \tag{53}$$

4.4. Boundary condition among cases

Consider the boundary between CASE M1 and CASE M2. At this boundary, the damping force just after each impulse in the steady state attains the relief force exactly. When each impulse acts at the point of zero restoring-force, the condition can be expressed by

$$\overline{V} + \overline{v}_c = \overline{V}_{DR} \Leftrightarrow \overline{V} = \overline{V}_{DR} - a_c\left(\equiv \overline{D}_c\right), \tag{54}$$

where $\overline{D}_c$ denotes the normalized input velocity level at the boundary between CASE M1 and CASE M2 and a_c can be obtained by Eq. (5).

On the other hand, when each impulse acts at the time when the velocity becomes maximum after each impulse, the condition can be expressed by

$$\overline{V} + \overline{v}_m = \overline{V}_{DR} \Leftrightarrow \overline{V} = \overline{V}_{DR} - a_m\left(\equiv \overline{D}_m\right), \tag{55}$$

where $\overline{D}_m$ denotes the normalized input velocity level at the boundary between CASE M1 and CASE M2 and a_m can be obtained by Eq. (31).

From Eqs. (54) and (55), if $\overline{V} \leq \overline{D}_c, \overline{D}_m$, the steady-state response is in CASE M1 and if $\overline{V} > \overline{D}_c, \overline{D}_m$ the steady-state response is in CASE M2.

Consider the boundary between CASE M2 and CASE M3. At this boundary, the maximum velocity before impulse in the steady state just attains the relief velocity and the condition can be expressed by

$$\overline{v}_m = \overline{V}_{DR} \Leftrightarrow \overline{V}_{DR} - a_m = \overline{D}_m = 0 \tag{56}$$

From Eq. (56), if $\overline{D}_m \geq 0$, the steady-state response is in CASE M2 and if $\overline{D}_m < 0$, the steady-state response is in CASE M3. The boundary input velocity level can be obtained by the relief velocity $\overline{V}_{DR}$ and the damping ratio h does not depend on input velocity level V. If $\overline{V}_{DR} > 1$, CASE M3 does not exist because $a_c < a_m < 1$ and

https://doi.org/10.1016/j.heliyon.2019.e01221

$\overline{D}_m < \overline{D}_c$ in the range $0 < h < 1$. In contrast, if CASE M3 exists, $\overline{D}_m \leq 0$ and CASE M1, in which each impulse acts at the maximum velocity timing, does not exist.

The boundaries between each CASE can be summarized as follows.

[Impulses act at the zero restoring-force timings]

CASE M1: $\overline{V} \leq \overline{D}_c$, CASE M2: $\overline{V} > \overline{D}_c$ and $\overline{D}_m \geq 0$, CASE M3: $\overline{D}_m < 0$,

[Impulses act at the maximum velocity timings]

CASE M1: $\overline{V} \leq \overline{D}_m$, CASE M2: $\overline{V} > \overline{D}_m$ and $\overline{D}_m \geq 0$, CASE M3: $\overline{D}_m < 0$,

5. Analysis

5.1. Accuracy check by time-history response analysis to multi impulse

The accuracy of the proposed solutions derived in Section 4 is investigated through the comparison with the critical steady-state response under the multi impulse calculated by time-history response analysis. Fig. 9(a)−(f) show the comparison of the critical steady-state response of the models with $V_{DR}/V_y = 0.5, 1.5, 2.5$ by the proposed closed-form solution with that by the time-history response analysis. The damping ratio of this system is $h = 0.15, 0.30$. In the legends of Fig. 9(a)−(f), "Approximation" means the response of the elastic perfectly-plastic SDOF model

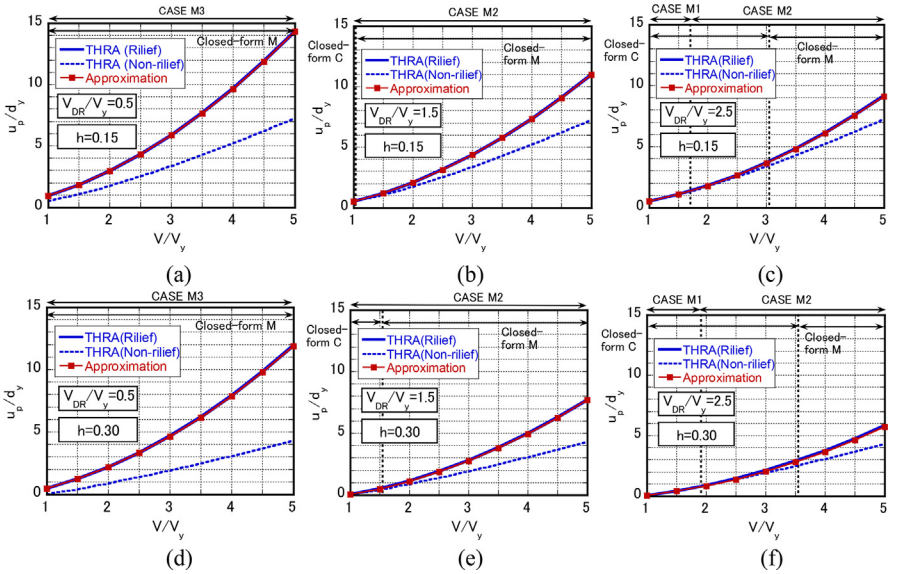

Fig. 9. Comparison of plastic deformation amplitude of model with nonlinear viscous damping under critical multi impulse by approximation with that by time-history response analysis, (a) $h = 0.15$, $V_{DR}/V_y = 0.5$, (b) $h = 0.15$, $V_{DR}/V_y = 1.5$, (c) $h = 0.15$, $V_{DR}/V_y = 2.5$, (d) $h = 0.30$, $V_{DR}/V_y = 0.5$, (e) $h = 0.30$, $V_{DR}/V_y = 1.5$, (f) $h = 0.30$, $V_{DR}/V_y = 2.5$.

https://doi.org/10.1016/j.heliyon.2019.e01221

with nonlinear viscous damping under the critical multi impulse by the proposed closed-form solution, "THRA(Relief)" indicates that by the time-history response analysis for the model with nonlinear viscous damping and "THRA(Non-relief)" means the response of the elastic perfectly-plastic SDOF model with linear viscous damping ($V_{DR}/V_y \to \infty$) under the critical multiple impulse by the time-history response analysis. The approximate closed-form solutions are obtained for the elastic perfectly-plastic SDOF model with nonlinear viscous damping under the multiple impulse in which each impulse acts at the zero restoring-force timing (Closed-form C) and the maximum velocity timing (Closed-form M), and the larger one is adopted as the critical steady-state response "Approximation". On the other hand, the critical steady-state response "THRA(Relief)" is evaluated by varying the time interval t_0 of the multiple impulse with constant input velocity level in time-history response analysis.

It can be observed from Fig. 9 that the proposed closed-form solution obtained in Section 4 can evaluate the plastic deformation amplitude under the multiple impulse despite of the relief velocity ratio V_{DR}/V_y and damping ratio h. The elastic-plastic response under the multi impulse such that each impulse acts at the zero-restoring force timing is adopted in the smaller input level and that under the multiple impulse such that each impulse acts at the maximum velocity timing is adopted in the larger input level as "Approximation" in Fig. 9. This result corresponds to the result in Section '**Maximum response of elastic perfectly-plastic SDOF model with nonlinear viscous damping under critical multi impulse'**.

5.2. Accuracy check by time-history response analysis subjected to the corresponding multi sine wave

The validity of the multi impulse as a substitute for the multi-cycle sine wave is investigated for the elastic perfectly-plastic SDOF model with nonlinear viscous damping and the accuracy of the proposed closed-form solution of the elastic-plastic system with nonlinear viscous damping is checked through the comparison with the steady-state response under the corresponding multi-cycle sine wave.

In the comparison of the elastic-plastic response under the multi impulse and the corresponding multi-cycle sine wave, Kojima and Takewaki (2015c, 2017) introduced the method tuning the level of both inputs based on the equivalence of the maximum Fourier amplitude, and this tuning method is also used in this paper. In this tuning method, the period of the corresponding sine wave is twice of the time interval of multi impulse. It is known that the response under impulse input becomes larger than that under sine wave in this model under the long-duration input. Therefore, in addition to the above tuning method ($\alpha = 1.00$), the acceleration amplitude of the sine wave is amplified by $\alpha = 1.15$ (Kojima and Takewaki, 2015c). The elastic-plastic response under the multi-cycle sine wave tuned based on the

https://doi.org/10.1016/j.heliyon.2019.e01221

equivalence of the maximum Fourier amplitude is denoted by "MSW" and that under the multi-cycle sine wave amplified by $\alpha = 1.15$ is denoted by "MSW $\times$ 1.15" in this section.

From the tuning method based on the equivalence of the maximum Fourier amplitude, the acceleration amplitude A_l and period $T_l(= 2\pi/\omega_l = 2t_0)$ of the corresponding sine wave can be calculated by following equations.

$$\frac{A_l}{V} = \frac{\alpha}{0.5t_0}, \tag{57}$$

$$\frac{V_l}{V} = \frac{\alpha}{0.5\pi}, \tag{58}$$

$$\omega_l = \frac{\pi}{t_0}, \tag{59}$$

where ω_l and V_l are the circular frequency and the velocity amplitude of the sine wave, and $\alpha = 1.00, 1.15$. ${t_0}^c/T_1$ for specific V/V_y, V_{DR}/V_y and h can be obtained by varying the time interval in time-history response analysis as shown in Fig. 3. ${t_0}^c$ is the critical timing between the two impulses which provides the maximum deformation and T_1 is the natural period of the elastic SDOF system.

The validity of the multi impulse as a substitute for the multi-cycle sine wave and the accuracy of the proposed solution for the steady-state response are investigated through the comparison with the response under the multi-cycle sine wave whose acceleration amplitude is tuned by using above method.

Fig. 10 shows the comparison of the plastic deformation amplitude of the model with $V_{DR}/V_y = 0.5, 1.5, 2.5$ under the critical multi impulse (MI) and that under the corresponding multi-cycle sine wave (MSW and MSW $\times$ 1.15). As in Fig. 9, "Approximation" means the response of the elastic perfectly-plastic SDOF model with nonlinear viscous damping under the critical multi impulse by the proposed closed-form solution, "THRA, Relief" indicates that by the time-history response analysis and "THRA, Non-relief" means the response of the elastic perfectly-plastic SDOF model with linear viscous damping ($V_{DR}/V_y \rightarrow \infty$) by the time-history response analysis. From Fig. 10, the response under the corresponding sine wave with $\alpha = 1.00$ (MSW) is smaller than that under the multi impulse (MI). This is because the decrease of the energy dissipation by relief mechanism under the multi impulse is larger than that under the sine wave and the damping force attains the relief force repeatedly under the long-duration ground motion. On the other hand, the plastic deformation amplitude by the proposed solution for the multi impulse (MI) and that under the corresponding sine wave with $\alpha = 1.15$ (MSW $\times$ 1.15) exhibit a fairly good correspondence. The effect of the velocity amplitude of the sine wave on the steady-state response of the model with nonlinear viscous

https://doi.org/10.1016/j.heliyon.2019.e01221

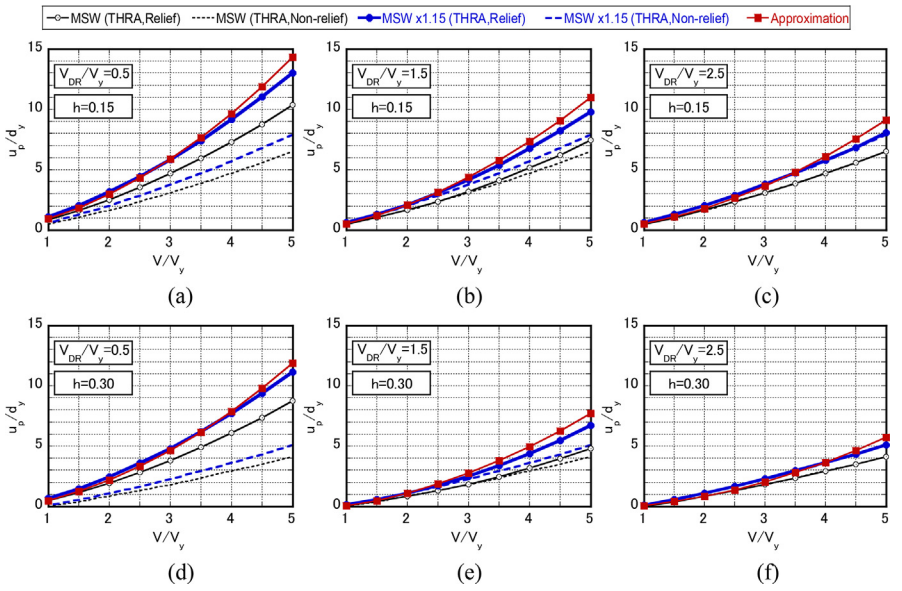

Fig. 10. Comparison of plastic deformation amplitude of model with nonlinear viscous damping under critical multi impulse (approximation) with that under corresponding multi-cycle sine wave (time-history response analysis), (a) $h = 0.15$, $V_{DR}/V_y = 0.5$, (b) $h = 0.15$, $V_{DR}/V_y = 1.5$, (c) $h = 0.15$, $V_{DR}/V_y = 2.5$, (d) $h = 0.30$, $V_{DR}/V_y = 0.5$, (e) $h = 0.30$, $V_{DR}/V_y = 1.5$, (f) $h = 0.30$, $V_{DR}/V_y = 2.5$.

damping is remarkable and the further investigation is necessary on the multiplier α of the acceleration amplitude of the sine wave. In the range of input velocity level $V/V_y < 3.0$, the multi impulse is a good substitute of the multi-cycle sine wave with $\alpha = 1.15$.

Figs. 9 and 10 are the plastic deformation amplitudes with respect to the input level. The common trend is that, while the model with linear damping (non-relief) exhibits smaller responses compared to the model with nonlinear damping (relief), the proposed approximate evaluation method shows a fairly good accuracy based on the comparison with the results by the time-history response analysis.

5.3. Accuracy check by time-history response analysis under recorded ground motion

The applicability of the proposed elastic-plastic response under the critical multi impulse to recorded long-duration ground motions is verified through the comparison with the response under the actual recorded ground motion. Tomakomai EW component during Tokachioki earthquake in 2003 is used as an actual long-duration ground motion. The velocity waveform of the long-duration and long-period ground motion can be represented approximately by the sine wave. A comparison of the ground velocity of Tomakomai EW (2003) and the equivalent sine wave is shown in Fig. 11.

https://doi.org/10.1016/j.heliyon.2019.e01221

Although the critical multi impulse is selected for the specific structure and the approximate closed-form solution is derived for the critical multi impulse in Sections 3 and 4, the parameters of the elastic-plastic system with nonlinear viscous damping is approximately determined to maximize the steady-state responses for the recorded ground motion with specific input velocity level in this section. In this paper, the method by Kojima et al. (2017) and Hayashi et al. (2018) is used in evaluating the critical response under the recorded ground motion.

First, the main part of the velocity waveform of the recorded ground motion is represented by the multi-cycle sine wave and the velocity amplitude V_l and period T_l of the equivalent sine wave are determined. The critical time interval ${t_0}^c$ can be obtained as a half of T_l here. The input velocity level V of the multi impulse corresponding to the multi-cycle sine wave can be obtained by using V_l and the multiplier α with the following equation.

$$V = 0.5\pi V_l/\alpha \tag{60}$$

Then ${t_0}^c/T$ for a specific set of V/V_y, V_{DR}/V_y and h is determined. It is necessary to obtain ${t_0}^c/T$ for a specific set of V/V_y, V_{DR}/V_y and h by varying the time interval in the time-history response analysis in advance, as shown Fig. 3. Finally, the parameters V_y, V_{DR}, ω_1 and d_y of the SDOF model can be obtained as follows with ${t_0}^c/T$, ${t_0}^c = 0.5T_l$ and Eq. (60).

$$V_y = \frac{V}{\left(V/V_y\right)}, \tag{61}$$

$$V_{DR} = \left(V_{DR}/V_y\right)V_y, \tag{62}$$

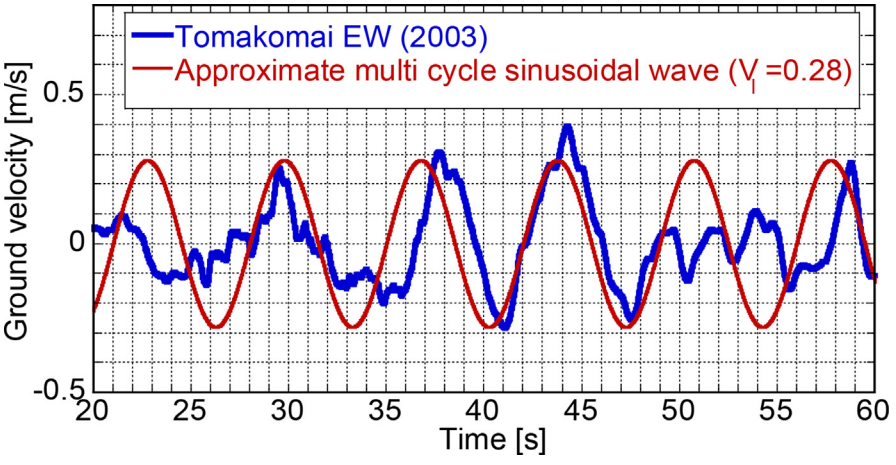

Fig. 11. Velocity wave of Tomakomai EW (2003) and the corresponding sine wave.

https://doi.org/10.1016/j.heliyon.2019.e01221

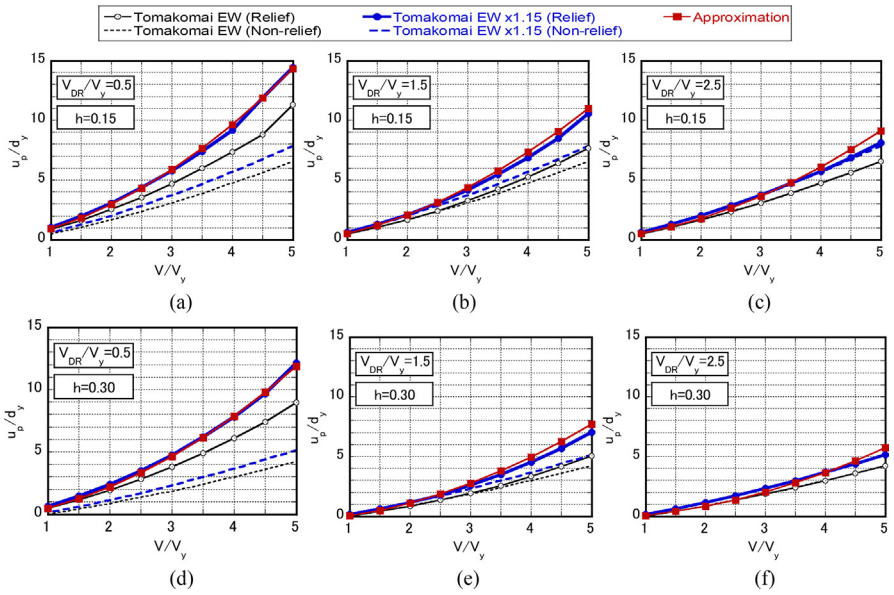

Fig. 12. Comparison of plastic deformation amplitude of model with nonlinear viscous damping under critical multi impulse (approximation) with that under recorded ground motion (time-history response analysis), (a) $h = 0.15$, $V_{DR}/V_y = 0.5$, (b) $h = 0.15$, $V_{DR}/V_y = 1.5$, (c) $h = 0.15$, $V_{DR}/V_y = 2.5$, (d) $h = 0.30$, $V_{DR}/V_y = 0.5$, (e) $h = 0.30$, $V_{DR}/V_y = 1.5$, (f) $h = 0.30$, $V_{DR}/V_y = 2.5$.

$$\omega_1 = \frac{2\pi\left(t_0^c/T_1\right)}{t_0^c}, \tag{63}$$

$$d_y = \frac{V_y}{\omega_1}, \tag{64}$$

The parameters of the SDOF model maximizing the elastic-plastic response under the actual recorded ground motion are determined by using the above procedure and the critical response under the multi impulse is compared with that under the actual recorded ground motion. The period of the equivalent multi-cycle sine wave is $T_l = 7.0$[sec] and the velocity of the equivalent sinusoidal wave is $V_l = 0.28$[m/sec]. Then the input velocity level of the multi impulse corresponding to the Tomakomai EW component is $V = 0.44$[m/sec]. V_l is determined so that the velocity amplitude of the multi-cycle sine wave corresponds to the amplitude of three wavelets of the ground velocity during 25−45 [sec] as shown in Fig. 11. Fig. 12 shows the comparison of plastic deformation amplitude of the model with nonlinear viscous damping under the critical multi impulse (designated as 'Approximation') with that under a recorded ground motion (time-history response analysis). For comparison, the response of the model with linear damping is provided as 'Non-relief'. As shown in Fig. 10, the case with an amplified coefficient 1.15 on the input intensity was also considered. It can be observed from Fig. 12 that the proposed elastic-plastic response under the critical multi impulse can simulate the critical elastic-plastic response under the recorded ground motion with $\alpha = 1.15$ within a

https://doi.org/10.1016/j.heliyon.2019.e01221

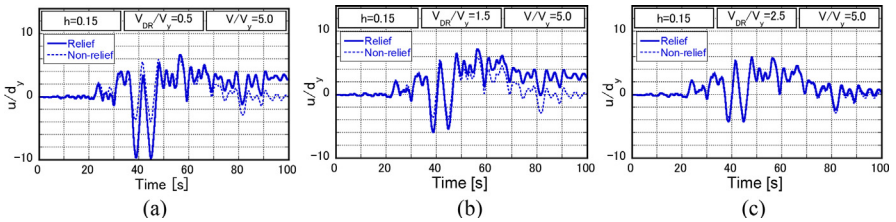

Fig. 13. Displacement response to Tomakomai EW (2003) for $V/V_y = 5.0$, (a) $h = 0.15$, $V_{DR}/V_y = 0.5$, (b) $h = 0.15$, $V_{DR}/V_y = 1.5$, (c) $h = 0.15$, $V_{DR}/V_y = 2.5$.

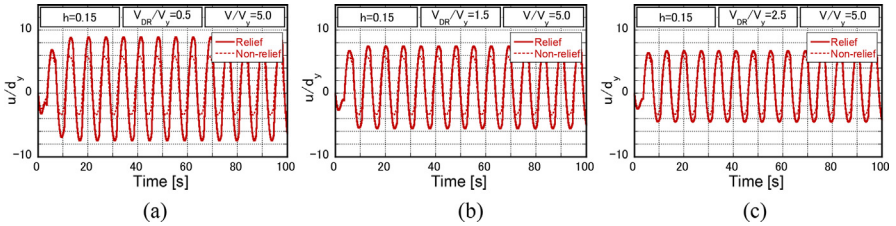

Fig. 14. Displacement response to critical multi impulse for $V/V_y = 5.0$, (a) $h = 0.15$, $V_{DR}/V_y = 0.5$, (b) $h = 0.15$, $V_{DR}/V_y = 1.5$, (c) $h = 0.15$, $V_{DR}/V_y = 2.5$.

reasonable accuracy. In addition, as in Figs. 9 and 10, while the model with linear damping (non-relief) exhibits smaller responses compared to the model with nonlinear damping (relief), the proposed approximate evaluation method shows a fairly good accuracy.

Figs. 13 and 14 show the comparison of the time-history displacement response of the model with $h = 0.15$, $V/V_y = 5.0$ and $V_{DR}/V_y = 0.5, 1.5, 2.5$ under the critical multi impulse and the recorded ground motion ($\alpha = 1.15$). It can be observed that the displacement response under the recorded ground motion is maximized in resonance with three wavelets during 25−45 [sec], and the difference between the displacement response of the models with and without relief mechanism is remarkable in this range.

6. Conclusions

Multi impulse has been employed as a substitute for long-duration ground motions and the critical steady-state response to that multi impulse has been investigated for an elastic-perfectly plastic SDOF model with nonlinear viscous damping. This simple model simulates the base-isolated building structure consisting of laminated natural rubber bearings, steel dampers and oil dampers with relief mechanism.

The conclusions may be summarized as follows.

(1) A closed-form solution has been obtained for the critical steady-state response of an elastic perfectly-plastic SDOF model with nonlinear viscous damping

https://doi.org/10.1016/j.heliyon.2019.e01221

under the multi impulse. While the critical timing for an elastic-plastic model with linear viscous damping is the zero restoring-force timing, it is the zero restoring-force timing in the lower input velocity level and shifts to the maximum velocity timing as the input velocity becomes larger for the elastic-plastic model including oil dampers with relief mechanism. The steady-state elastic-plastic responses have been derived for two cases, (i) each impulse acts at the zero restoring-force timing, (ii) each impulse acts at the maximum velocity timing. Then the larger one has been adopted as the critical steady-state response. In the derivation of the critical steady-state responses, the quadratic or elliptical function approximations has been used for approximating the damping force-deformation relation. The elliptical approximation of the curved part in the damping force-deformation relation has been used to obtain the maximum velocity in the stage where the damping force is constant as the relief force. The quadratic function approximation and the energy balance law have been used for deriving the plastic deformation amplitude.

(2) The time-history response analysis to the multi impulse demonstrated that the proposed closed-form solution can approximately evaluate the steady-state response of the elastic perfectly-plastic SDOF model with nonlinear viscous damping under the critical multi impulse.

(3) The comparison with the time-history response analysis result for the elastic-plastic response under the amplitude-tuned multi-cycle sine wave confirmed the validity of the proposed closed-form solution. It was made clear that, to adjust the response under the multi impulse and the corresponding multi-cycle sine wave, it is necessary to amplify the acceleration amplitude of the multi-cycle sine wave by 1.15 after it is tuned so that the maximum Fourier amplitude of the multi-cycle sine wave is equal to that of the multi impulse. This is because the impulse input gives instantaneous change of velocity of mass and the responses under the impulse input are amplified larger than that under the sine wave.

(4) It has been shown through the comparison with a linear viscous damping model that the nonlinearity in viscous damping causes a remarkable influence on the earthquake response in some cases.

(5) The applicability of the proposed solutions has been investigated through the comparison with the elastic-plastic response under a recorded long-duration ground motion. The velocity of the recorded ground motion is modeled by the multi-cycle sine wave and it is further transformed into the multi impulse. The proposed solution for the critical multi impulse exhibits good correspondence with that under the recorded long-duration ground motion.

https://doi.org/10.1016/j.heliyon.2019.e01221

Declarations

Author contribution statement

Goki Tamura: Conceived and designed the experiments; Performed the experiments; Analyzed and interpreted the data; Wrote the paper.

Kotaro Kojima: Analyzed and interpreted the data; Wrote the paper.

Izuru Takewaki: Conceived and designed the experiments; Analyzed and interpreted the data; Wrote the paper.

Funding statement

This work was supported by KAKENHI of Japan Society for the Promotion of Science (No. 15H04079, 17J00407, 17K18922, 18H01584)

Competing interest statement

The authors declare no conflict of interest.

Additional information

No additional information is available for this paper.

References

Akehashi, H., Kojima, K., Takewaki, I., 2018. Critical response of SDOF damped bilinear hysteretic system under double impulse as substitute for near-fault ground motion. Front. Built Environ. 4, 5.

Aoi, S., Honda, R., Morikawa, N., Sekiguchi, H., Suzuki, H., Hayakawa, Y., Kunugi, T., Fujiwara, H., 2008. Three-dimensional finite difference simulation of long-period ground motions for the 2003 Tokachi-oki, Japan, earthquake. J. Geophys. Res. 113, B07302.

Beck, J.L., Hall, J.F., 1986. Factors contributing to the catastrophe in Mexico City during the earthquake of September 19, 1985. Geophys. Res. Lett. 13 (6), 593−596.

Caughey, T.K., 1960a. Sinusoidal excitation of a system with bilinear hysteresis. J. Appl. Mech. 27, 640−643.

Caughey, T.K., 1960b. Random excitation of a system with bilinear hysteresis. J. Appl. Mech. 27, 649−652.

https://doi.org/10.1016/j.heliyon.2019.e01221

Domenico, D.D., Ricciardi, G., Takewaki, I., 2019. Design strategies of viscous dampers for seismic protection of building structures: a review. Soil Dynam. Earthq. Eng. (in press).

Fujita, K., Yasuda, K., Kanno, Y., Takewaki, I., 2017. Robustness evaluation of elastic-plastic base-isolated high-rise buildings under critical double impulse. Front. Built Environ. 3, 31.

Furumura, T., Hayakawa, T., 2007. Anomalous propagation of long-period ground motions recorded in Tokyo during the 23 October 2004 Mw 6.6 Niigata-ken Chuetsu, Japan, earthquake. Bull. Seismol. Soc. Am. 97 (3), 863−880.

Hatayama, K., Zama, S., Nishi, H., Yamada, M., Hirokawa, Y., Inoue, R., 2004. Long-period strong ground motion and damage to oil storage tanks due to the 2003 Tokachi-oki Earthquake. Zisin 57 (2), 83−103 (in Japanese).

Hayashi, K., Fujita, K., Tsuji, M., Takewaki, I., 2018. A simple response evaluation method for base-isolation building-connection hybrid structural system under long-period and long-duration ground motion. Front. Built Environ. 4, 2.

Iwan, W.D., 1961. The Dynamic Response of Bilinear Hysteretic Systems. Ph.D. Thesis. California Institute of Technology, Pasadena.

Iwan, W.D., 1965a. The dynamic response of the one-degree-of-freedom bilinear hysteretic system. In: Proc. of the Third World Conf. on Earthquake Eng., New Zealand.

Iwan, W.D., 1965b. The steady-state response of a two-degree-of-freedom bilinear hysteretic system. J. Appl. Mech. 32 (1), 151−156.

Kojima, K., Takewaki, I., 2015a. Critical earthquake response of elastic-plastic structures under near-fault ground motions (Part 1: fling-step input). Front. Built Environ. 1, 12.

Kojima, K., Takewaki, I., 2015b. Critical earthquake response of elastic-plastic structures under near-fault ground motions (Part 2: forward-directivity input). Front. Built Environ. 1, 13.

Kojima, K., Takewaki, I., 2015c. Critical input and response of elastic-plastic structures under long-duration earthquake ground motions. Front. Built Environ. 1, 15.

Kojima, K., Takewaki, I., 2016. Closed-form critical earthquake response of elastic-plastic structures with bilinear hysteresis under near-fault ground motions. J. Struct. Constr. Eng. AIJ 726, 1209−1219 (in Japanese).

https://doi.org/10.1016/j.heliyon.2019.e01221

Kojima, K., Takewaki, I., 2017. Critical steady-state response of single-degree-of-freedom bilinear hysteretic system under multi impulse as substitute of long-duration ground motion. Front. Built Environ. 3, 41.

Kojima, K., Saotome, Y., Takewaki, I., 2017. Critical earthquake response of a SDOF elastic-perfectly plastic model with viscous damping under double impulse as a substitute of near-fault ground motion. J. Struct. Construction Eng. AIJ 735, 643−652 (in Japanese), [English Version] Japan Architectural Review, Wiley, 2018.

Kubo, K., Hisada, Y., Horiuchi, S., Yamamoto, S., 2009. Application of long-period ground motion prediction using earthquake early warning system to elevator emergency operation control system of a high-rise building. J. Jpn. Assoc. Earthq. Eng. 9 (2), 31−50 (in Japanese).

Liu, C.-S., 2000. The steady loops of SDOF perfectly elastoplastic structures under sinusoidal loadings. J. Mar. Sci. Technol. 8, 50−60.

Losanno, D., Spizzuoco, M., Serino, G., 2014. Optimal design of seismic isolation systems for simply supported bridges. Earthq. Struct. 7 (6), 969−999.

Losanno, D., Spizzuoco, M., Serino, G., 2015. An optimal design procedure for a simple frame equipped with elastic-deformable dissipative braces. Eng. Struct. 101, 677−697.

Losanno, D., Hadad, H.A., Serino, G., 2017. Seismic behavior of isolated bridges with additional damping under far-field and near fault ground motion. Earthq. Struct. 13 (2), 119−130.

Motosaka, M., Mitsuji, K., 2012. Building damage during the 2011 off the Pacific coast of Tohoku earthquake. Soils Found. 52 (5), 929−944.

Roberts, J.B., Spanos, P.D., 1990. Random Vibration and Statistical Linearization. Wiley, New York, NY.

Takewaki, I., Murakami, S., Fujita, K., Yoshitomi, S., Tsuji, M., 2011. The 2011 off the Pacific coast of Tohoku earthquake and response of high-rise buildings under long-period ground motions. Soil Dynam. Earthq. Eng. 31 (11), 1511−1528.

Takewaki, I., Tsujimoto, H., 2011. Scaling of design earthquake ground motions for tall buildings based on drift and input energy demands. Earthq. Struct. 2, 171−187.

Takewaki, I., Moustafa, A., Fujita, K., 2012. Improving the Earthquake Resilience of Buildings: the Worst Case Approach. Springer, London.

https://doi.org/10.1016/j.heliyon.2019.e01221

Takewaki, I., Taniguchi, R., Kojima, K., 2017. Critical response of elastic-plastic structures to near-fault ground motions and its application to base-isolated building structures, Chapter 6, "*International Symposium in Earthquake Engineering and Structural Dynamics*" in memory of late Professor Ragnar Sigbjörnsson. In: Conference in Reykjavik - June 2017, (Earthquake Engineering and Structural Dynamics in Memory of Ragnar Sigbjörnsson, pp. 123−141.

Taniguchi, R., Kojima, K., Takewaki, I., 2016. Critical response of 2DOF elastic-plastic building structures under double impulse as substitute of near-fault ground motion. Front. Built Environ. 2, 2.

Tsuji, M., Tanaka, H., Yoshitomi, S., Takewaki, I., 2012. Optimum relief force of oil dampers in multi-story buildings. J. Struct. Constr. Eng. AIJ 678, 1237−1246 (in Japanese).

https://doi.org/10.1016/j.heliyon.2019.e01221